

Supplementary Information for

Local spectroscopy of moiré-induced electronic structure in gate-tunable twisted bilayer graphene

Dillon Wong, Yang Wang, Jeil Jung, Sergio Pezzini, Ashley M. DaSilva, Hsin-Zon Tsai, Han Sae Jung, Ramin Khajeh, Youngkyou Kim, Juwon Lee, Salman Kahn, Sajjad Tollabimazraehno, Haider Rasool, Kenji Watanabe, Takashi Taniguchi, Alex Zettl, Shaffique Adam, Allan H. MacDonald, Michael F. Crommie

Table of Contents

- 1. Atomic lattice and moiré superlattices**
- 2. Super-superlattice of twisted bilayer graphene on a BN substrate**
- 3. dI/dV spectra of coexisting moiré patterns**
- 4. dI/dV spectra on different regions of moiré pattern**
- 5. Gate-dependent dI/dV spectra on tBLG**
- 6. Theoretical moiré band structure plots of tBLG with different twist angles**
- 7. Theoretical calculations for different values of Fermi velocity**
- 8. Scaling behavior of spectroscopic features**

1. Atomic lattice and moiré superlattices

Fig. S1 shows a magnified version of the same image shown in Fig. 1b of the main text so that the atomic lattice can be seen more clearly.

2. Super-superlattice of twisted bilayer graphene on a BN substrate

As mentioned in the main text, when the wavelengths of the graphene-graphene moiré (λ_{g-g}) and graphene-BN moiré (λ_{g-BN}) are nearly equal, their periodicities can beat together to form a larger moiré pattern of the composite moirés. This type of super-superlattice structure is shown in Fig. 1d of the main text, and an atomically resolved topographic image of the same structure is depicted Fig. S2a. We use a Fourier transform (Fig. S2b) to obtain $\lambda_{g-BN} = 4.7$ nm, $\lambda_{g-g} = 4$ nm, and the rotation angle between the

graphene-graphene moiré and the graphene-BN moiré $\Delta\theta = 18^\circ$. These factors are input into the following equation for the super-superlattice period:

$$\lambda_S = \frac{\lambda_{g-BN}}{\sqrt{\left(\frac{\lambda_{g-BN}}{\lambda_{g-g}}\right)^2 + 1 - 2\left(\frac{\lambda_{g-BN}}{\lambda_{g-g}}\right)\cos(\Delta\theta)}}$$

This yields $\lambda_S = 12$ nm, consistent with direct measurement of the super-superlattice periodicity in Fig. 1d of the main text.

Fig. 1d of the main text is replicated in Fig. S2c, but with additional guidelines to highlight the directions of the various periodicities: the black guideline follows the graphene-graphene moiré pattern, the white guideline follows the graphene-BN moiré pattern, and the purple line follows the super-superlattice moiré pattern.

3. dI/dV spectra of coexisting moiré patterns

In the main text, we show dI/dV spectra taken on regions of our tBLG/BN device with large $\theta_{g-BN} > 15^\circ$. In Fig. S2d, we show dI/dV spectra taken on the regions shown in Figs 1b-d of the main text (where $\theta_{g-BN} < 15^\circ$). These spectra show features induced by the graphene-graphene moiré pattern (namely, the VHS peak and the following dip), but not any features induced by the graphene-BN moiré pattern (such as graphene-BN superlattice Dirac points).

4. dI/dV spectra on different regions of moiré pattern

In Fig. 3 of the main text, we show dI/dV spectra taken in the AA regions of tBLG moiré patterns. Fig. S3 shows dI/dV spectra taken in different regions of the graphene-graphene moiré pattern. The black curve is taken on the AA region, the red curve is taken on the bridge region, and the green curve is taken on the AB/BA region (see Fig. 2c of the main text for the definition of these regions).

In order to better visualize the spatial distribution of the LDOS of tBLG at different energies, we acquired a dI/dV spectral grid on tBLG for $\lambda_{g-g} = 7.6$ nm. dI/dV maps of tBLG at the energies of the different spectral features (extracted from the same spectral grid) are shown in Fig. S4, together with the corresponding theoretical

simulations. The dI/dV maps show a clear trend in the distribution of the dI/dV intensity across the moiré pattern. The dI/dV signal is strongest in the AA regions at the energies of the VHS peak and the 1st dip, while most of the dI/dV weight shifts to the AB/BA regions at the energy of the 2nd dip. The observed evolution of the distribution of the LDOS over the moiré pattern is consistent with the theoretical simulations. This behavior can be understood within the framework of moiré bands: as the energy transits from the first moiré band to the second moiré band, the wave function gains an extra phase of $\pi/2$ due to the band folding and thus switches the positions of its nodes.

5. Gate-dependent dI/dV spectra on tBLG

The gate-tunability of our tBLG/BN devices is important for accurate energy measurements. Gate-dependent dI/dV spectra acquired in the AA region of a 7.6 nm graphene-graphene moiré pattern are shown in Fig. S5. All of the features (VHS peak, 1st dip, and 2nd dip) shift with the gate-induced doping in a similar way as the Dirac point, but the measured energy differences between different features change slightly with the graphene doping level (see Fig. S6). The solid symbols in Fig. S6 represent data points measured when the tBLG is highly doped by the back-gate (either $V_g = +60$ V or $V_g = -60$ V), while the hollow symbols represent data points measured when the sample is close to neutral ($V_g \approx 0$ V). The energies measured under the neutral condition are slightly larger than those measured under the highly doped condition.

This systematic difference can be explained by tip-induced band bending (TIBB). When the tBLG is nearly neutral, the TIBB effect is large because $\text{DOS}(E_F)$ is small, and the measured feature voltages are then magnified (due to TIBB) compared to their true values. On the other hand, the influence of TIBB is significantly reduced when the tBLG is heavily doped and $\text{DOS}(E_F)$ is large. Therefore, the feature energies measured under the highly doped condition are systematically smaller than the ones measured under the neutral condition and more accurately reflect the true DOS energies (since there is less TIBB). The gating capability of our device is thus important for increasing the measurement accuracy of the spectroscopic feature energies of tBLG.

6. Theoretical moiré band structure plots of tBLG with different twist angles

Calculated moiré band structure plots of tBLG are displayed in Fig. S7 for twist angles beyond what is shown in the main text. This series of band structure plots demonstrates the transition from the perturbative regime (large twist angle and small moiré pattern) to the non-perturbative regime (small twist angle and large moiré pattern). One signature of this transition is that the size of the partial band gap between different moiré bands relative to the corresponding bandwidth increases dramatically as the twist angle decreases.

7. Theoretical calculations for different values of Fermi velocity

The only adjustable parameter in our theory (see Jung *et al. PRB* **89**, 205414 (2014) for more details) is the unperturbed graphene Fermi velocity, which we take to be $v_F = 1.05 \times 10^6$ m/s. Fig. S8 shows our experimental data juxtaposed with the same calculation for different values of v_F beyond what is shown in the main text. As can be seen in Fig. S8c, $v_F = 1.05 \times 10^6$ m/s fits the experimental data quite well.

8. Scaling behavior of spectroscopic features

Unlike the VHS peak, $1/\lambda_{g-g}$ scaling is not preserved for large moiré periods for the 1st dip. Fig. S9a plots the experimental energies of the VHS peak and 1st dip against $1/\lambda_{g-g}$ together with straight lines as guides to the eye. In contrast to the VHS energy (which follows a straight line when plotted against $1/\lambda_{g-g}$), the 1st dip energy deviates from straight-line behavior for $1/\lambda_{g-g} < 0.2 \text{ nm}^{-1}$ (or $\lambda_{g-g} > 5 \text{ nm}$). This is a signature of the non-perturbative nature of the graphene-graphene interlayer interaction.

Another way to represent the non-perturbative nature of the graphene-graphene interlayer interactions is displayed in Fig. S9b. Here we plot (for various λ_{g-g}) the ratio of the experimental 1st dip energy to the VHS energy and the ratio of the 2st dip energy to the 1st dip energy. The energy ratios remain reasonable constant for $\lambda_{g-g} < 5 \text{ nm}$ before rapidly changing in the large moiré regime, indicative of a strongly non-perturbative interaction.

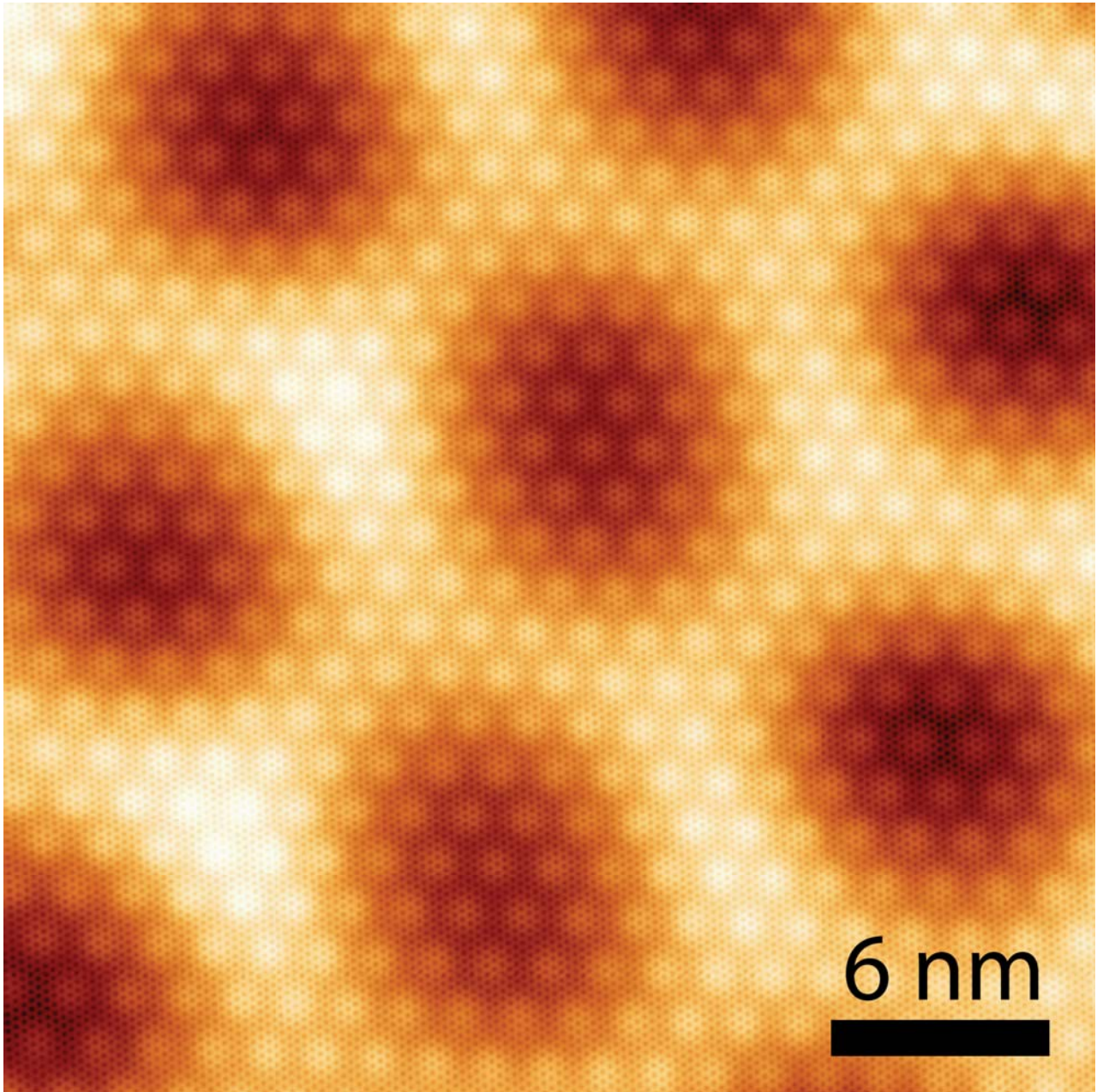


Figure S1. Multiple length scales in a tBLG/BN device. Magnified version of Fig. 1b of the main text. The atomic lattice, graphene-graphene moiré pattern, and graphene-BN moiré pattern are all visible in this image.

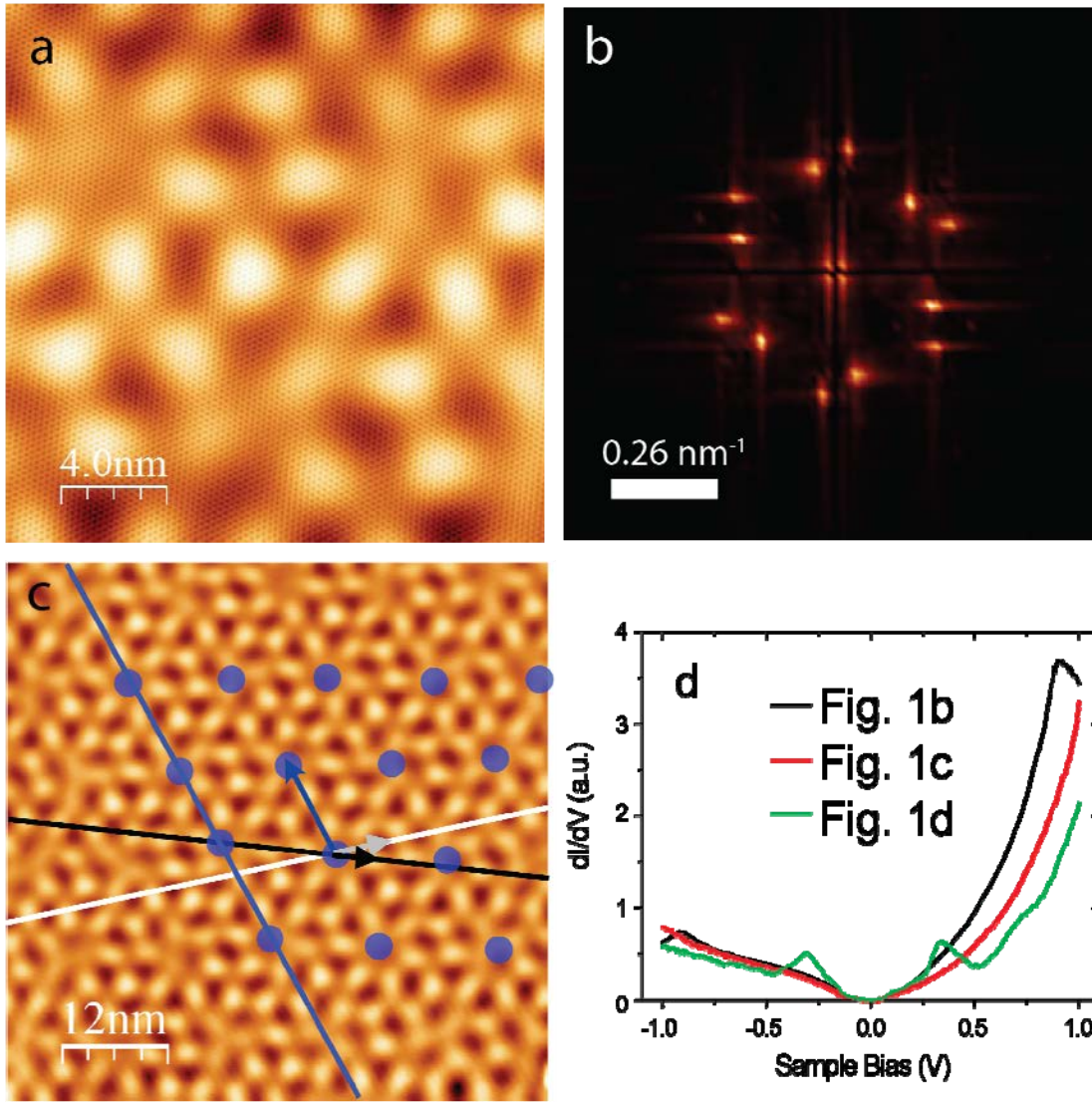


Figure S2. Super-superlattice of tBLG on BN. (a) Atomsically resolved STM topographical image ($V_s = -0.15$ V, $I = 0.3$ nA) shows zoom-in of super-superlattice displayed in Fig. 1d of the main text. (b) Fourier transform of Fig. 1d of the main text. The spots represent the graphene-graphene and graphene-BN moiré patterns. (c) Same as Fig. 1d but with additional superimposed guidelines showing moiré pattern directions: black line for graphene-graphene moiré, white line for graphene-BN moiré, and purple line for super-superlattice moiré. (d) dI/dV spectra ($V_s = -1$ V, 0.3 nA $\leq I \leq 0.5$ nA, $V_g = 0$ V, a.c. modulation $V_{rms} = 6$ mV) taken in the areas shown in Figs 1b-d of the main text.

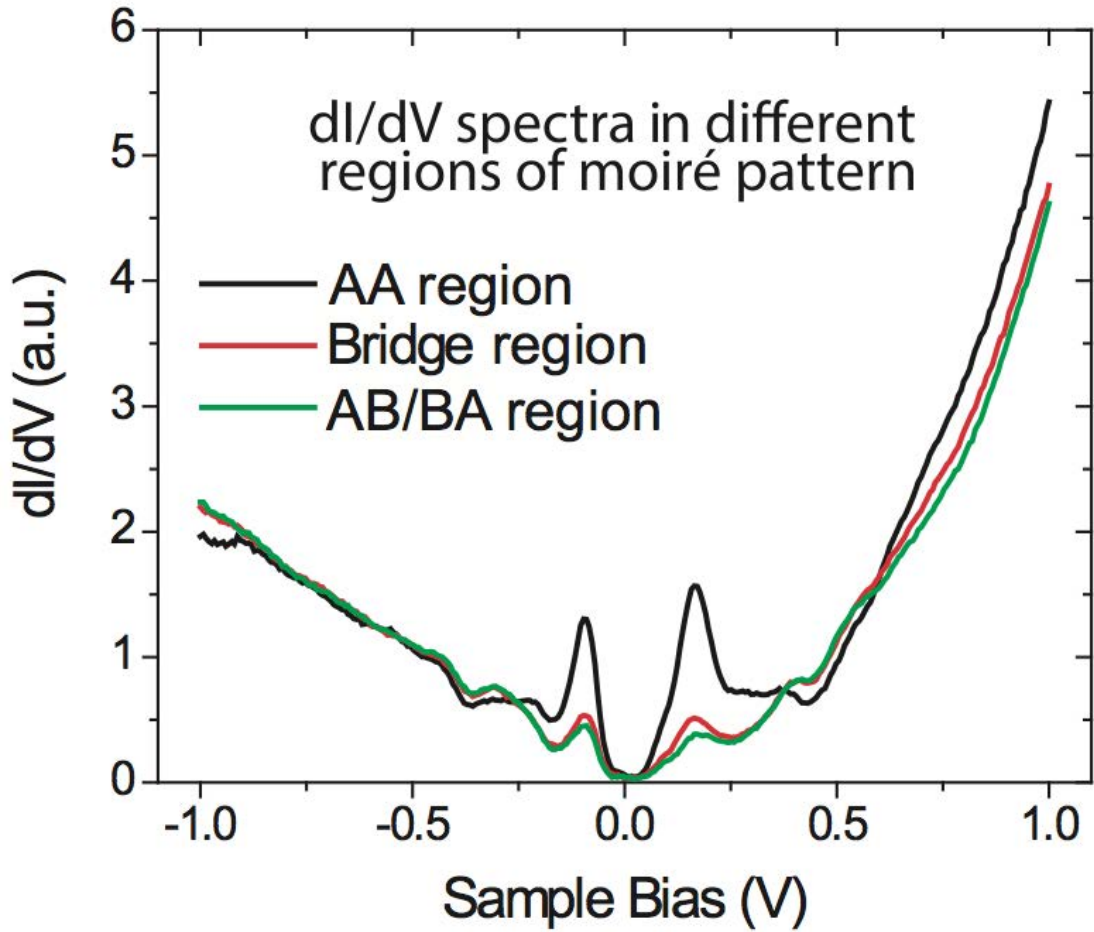


Figure S3. STM dI/dV spectra measured in different regions of the graphene-graphene moiré pattern having $\lambda_{g-g} = 7.6$ nm. The black curve is taken in the AA region, the red curve is taken in the bridge region, and the green curve is taken in the AB/BA region (see Fig. 2c of the main text for the definition of the regions). Initial tunneling parameters: $V_s = -1$ V, $I = 0.4$ nA, $V_g = 0$ V, a.c. modulation $V_{rms} = 6$ mV.

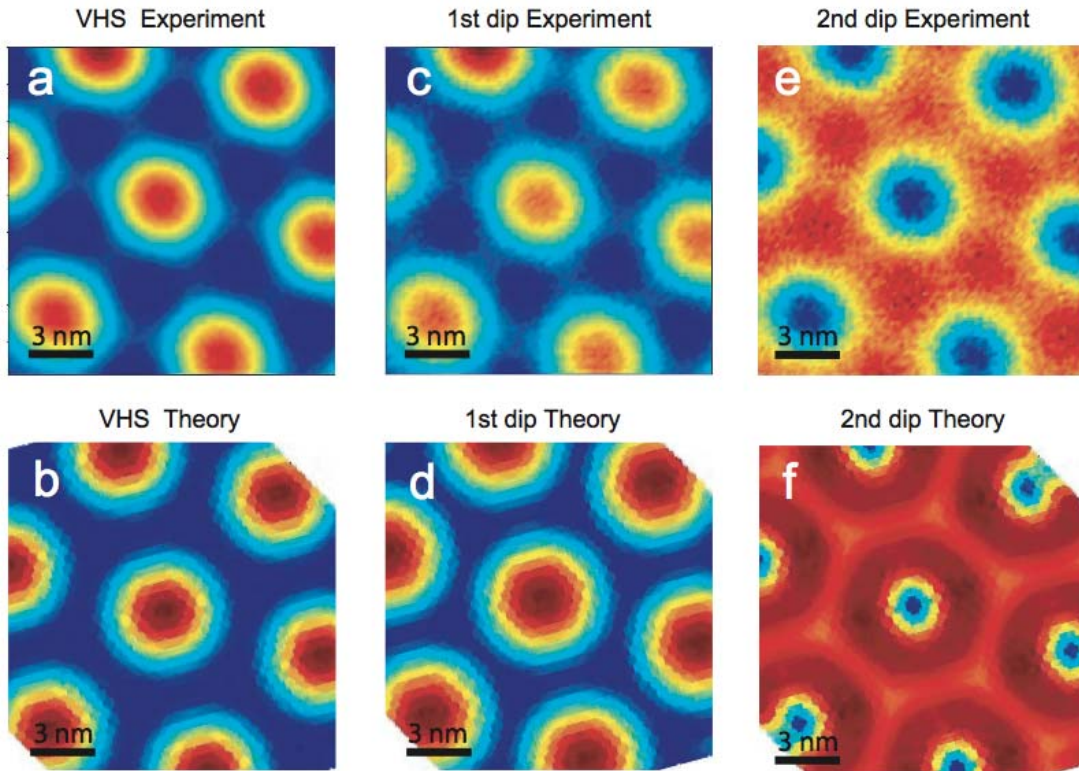


Figure S4. Comparison between experimental and theoretical dI/dV maps at the energies of the VHS peak, 1st dip, and 2nd dip. (a) Experimental STM dI/dV map (from spectral grid) at the energy of the VHS peak (-87.5 meV) of tBLG with moiré size $\lambda_{g-g} = 7.6$ nm. Initial tunneling parameters: $V_s = -0.7$ V, $I = 0.6$ nA, $V_g = -10$ V, a.c. modulation $V_{rms} = 8$ mV. (b) Theoretically simulated LDOS at the energy of the VHS peak of tBLG having moiré size $\lambda_{g-g} = 7.6$ nm. (c) Same region as in a except taken at the energy of the 1st dip (-143.8 meV). (d) Same as in b except at the energy of the 1st dip. (e) Same region as in a except taken at the energy of the 2nd dip (-350 meV). (f) Same as in b except at the energy of the 2nd dip.

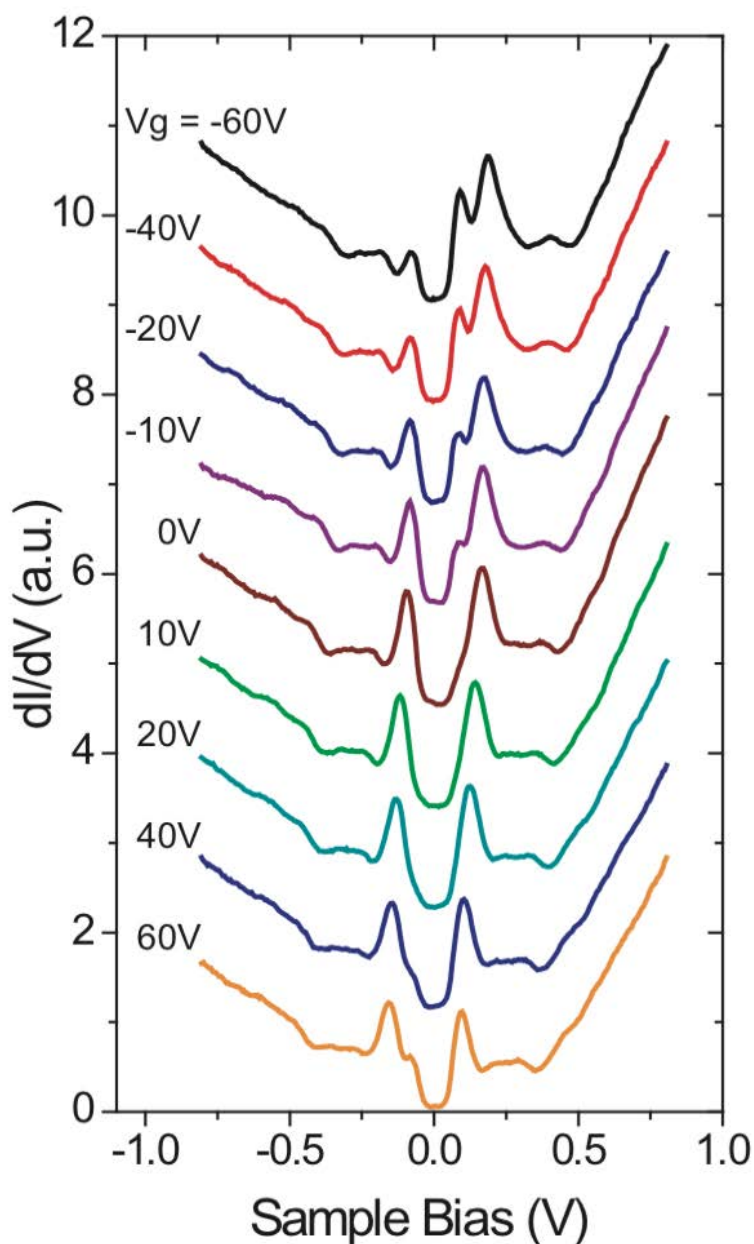


Figure S5. Gate-dependent STM dI/dV spectra taken in the tBLG AA region of a $\lambda_{g-g} = 7.6$ nm graphene-graphene moiré pattern. All of the features (VHS peak, 1st dip, and 2nd dip) shift with carrier doping in a similar way as the Dirac point. Initial tunneling parameters: $V_s = -1$ V, $I = 0.40$ nA, a.c. modulation $V_{\text{rms}} = 6$ mV. Curves are shifted vertically for clarity.

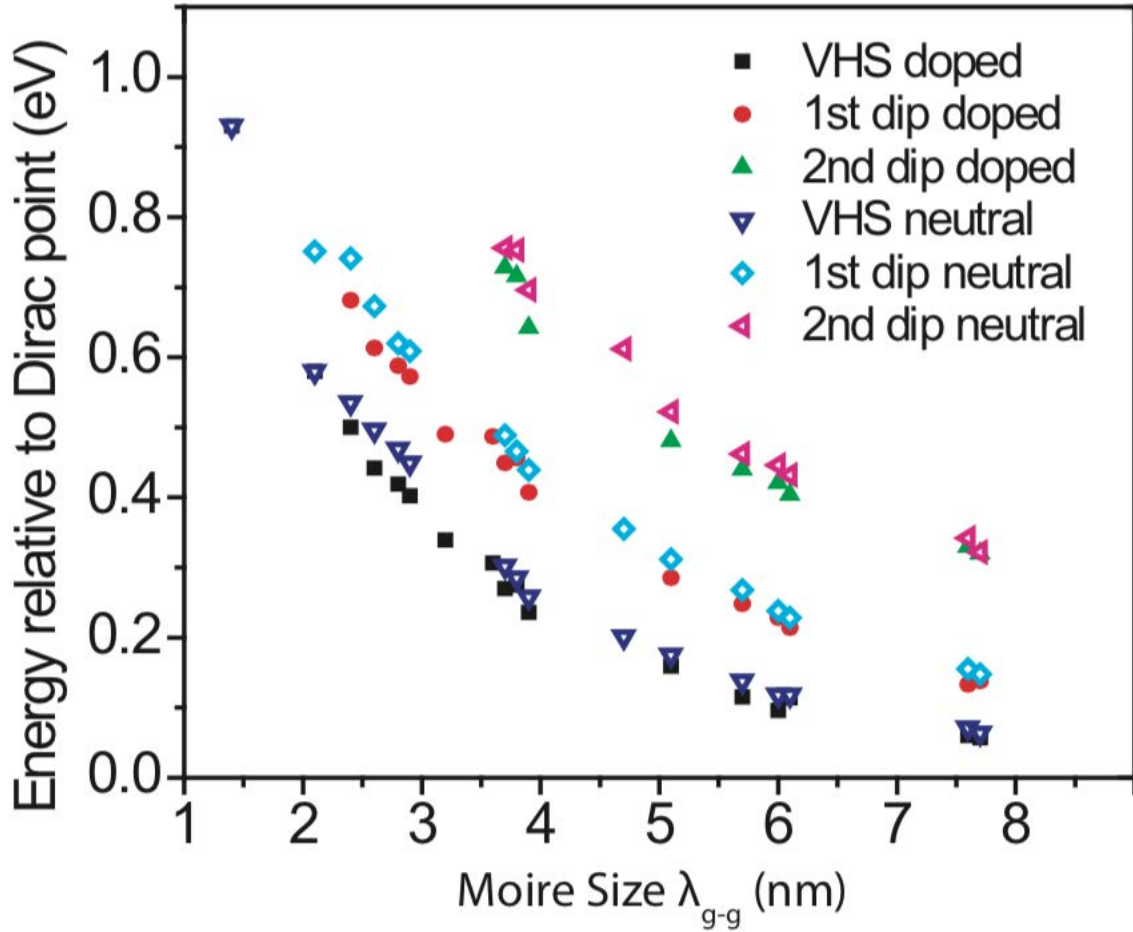


Figure S6. Comparison of the spectroscopic feature energies measured under different doping conditions as a function of moiré size. The solid symbols represent data points measured when the twisted bilayer graphene is highly doped by the back-gate ($V_g = \pm 60$ V), while the hollow symbols represent data points measured when the sample is close to neutral. There is a systematic difference between the data measured under these two conditions. The energies measured under the neutral condition are slightly larger than those measured under the highly doped condition due to tip induced band bending. The energy magnitudes plotted here are all measured relative to the Dirac point.

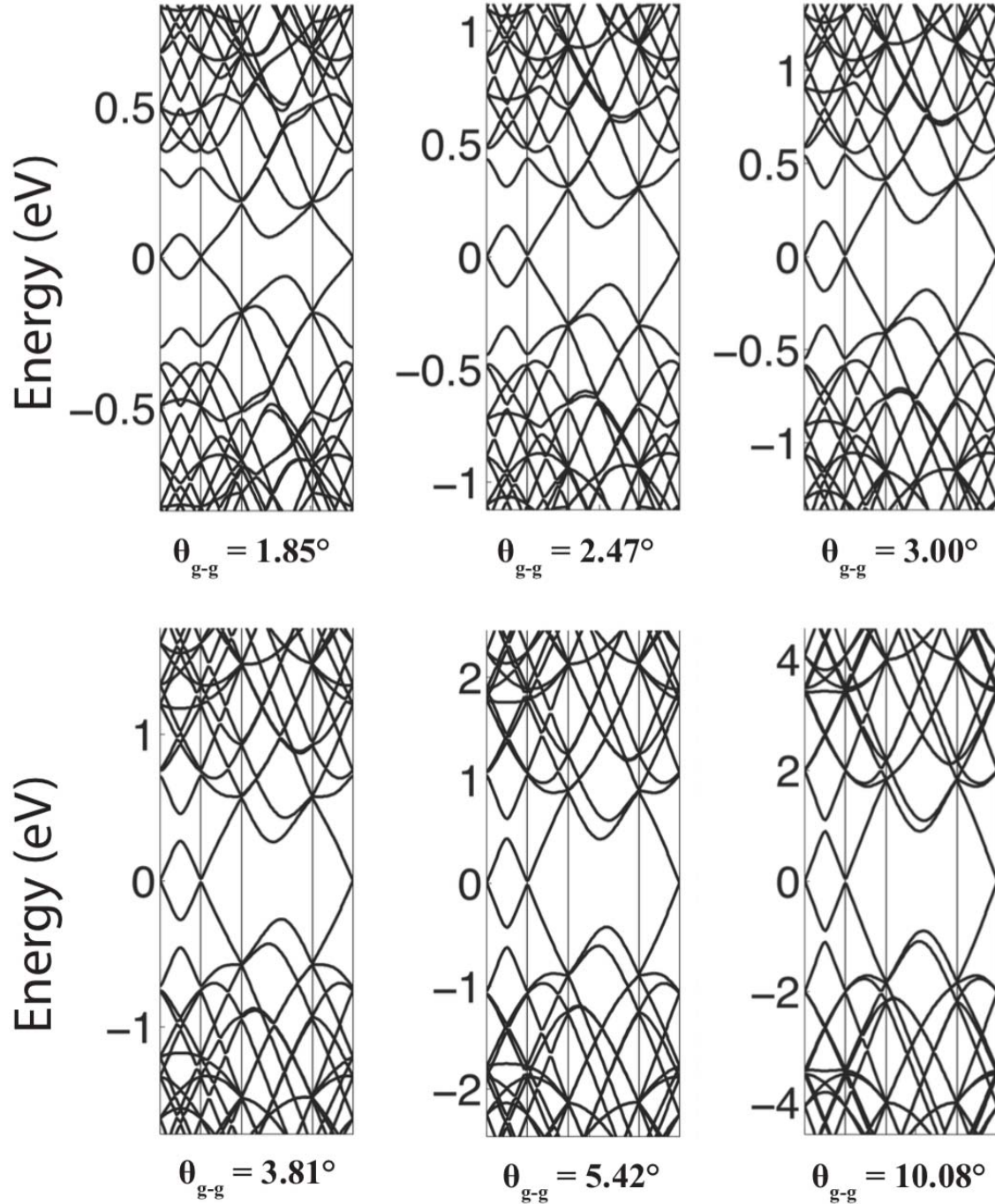


Figure S7. Calculated moiré band structure plots of tBLG for different graphene-graphene twist angles. The set of twist angles chosen corresponds to moiré wavelengths 7.6 nm, 5.7 nm, 4.7 nm, 3.7 nm, 2.6 nm and 1.4 nm. Each band structure plot is drawn in a similar fashion as Fig. 4c of the main text.

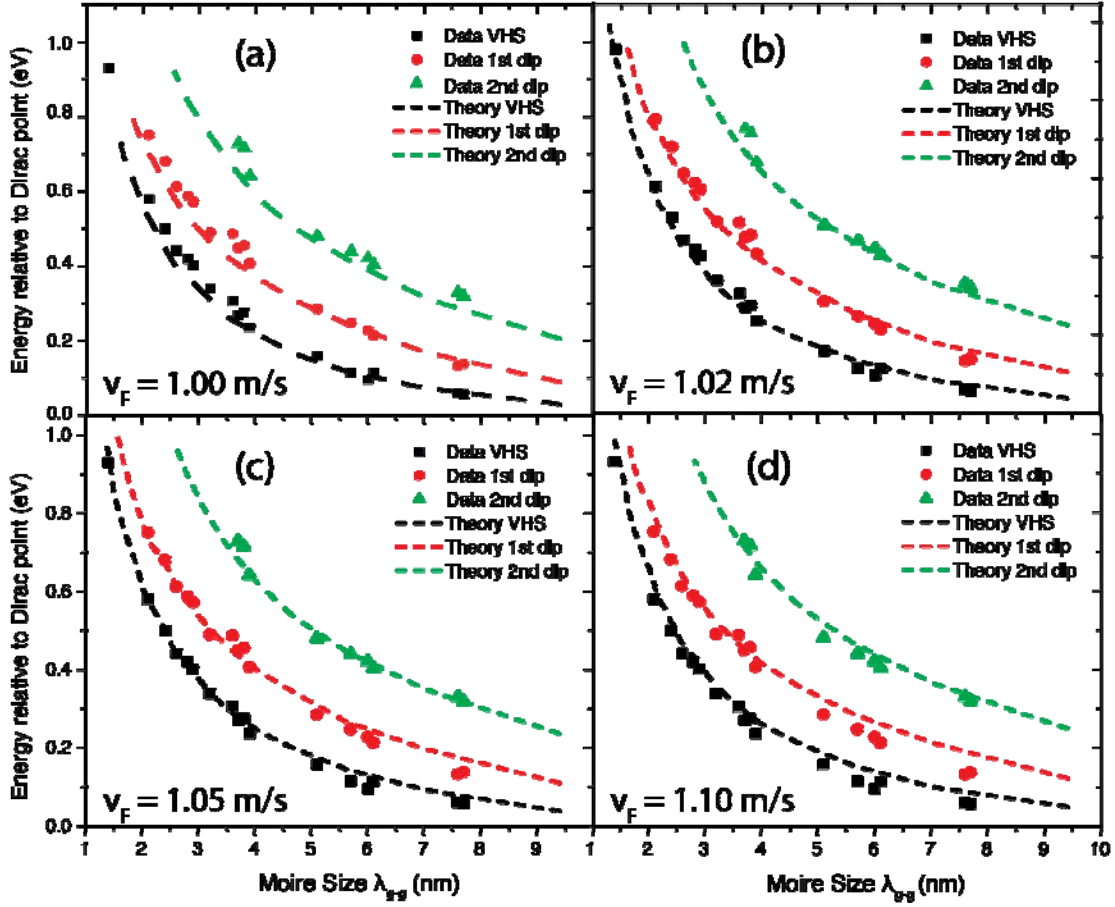


Figure S8. Theoretical calculations of VHS peak, 1st dip, and 2nd dip energies for different Fermi velocities. The only adjustable parameter in our theory is the unperturbed monolayer graphene Fermi velocity v_F . Here we show theoretical calculations (dashed lines) superimposed on experimental data (scattered dots) for different values of v_F .

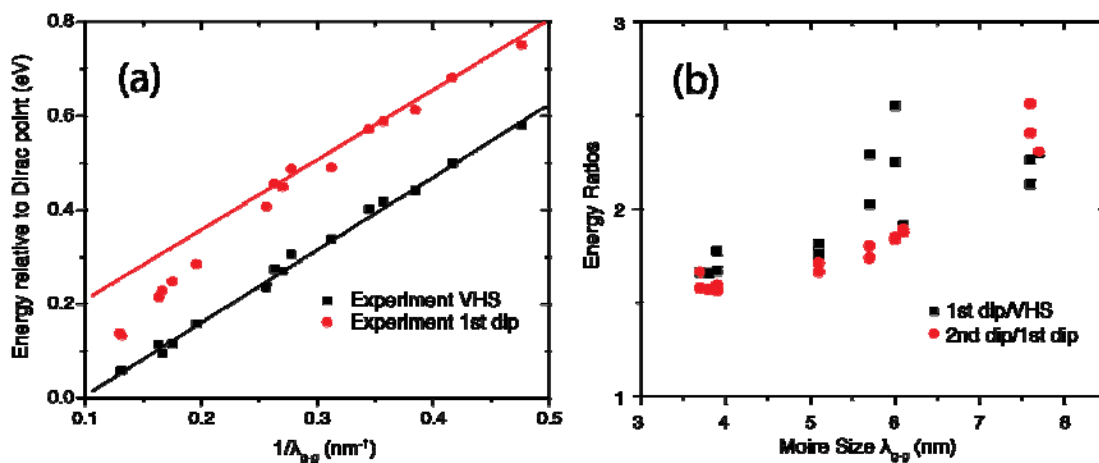


Figure S9. First dip in tBLG spectroscopy deviates from $1/\lambda_{gg}$ scaling for large graphene-graphene moiré periods. (a) Experimental VHS peak and 1st dip energies plotted against $1/\lambda_{gg}$ (with straight lines shown as guides to the eye). (b) Experimental 1st dip energy/VHS energy (black squares) and 2nd dip energy/1st dip energy (red circles) ratios for different moiré sizes.